CHEMISTRY
A European Journal

www.chemeurj.org

A Journal of ChemPubSoc Europe

Reprint

ACES Asian Chemical Editorial Society

WILEY-VCH

ChemPubSoc Europe
DOI: 10.1002/chem.201901034
CHEMISTRY A European Journal
Full Paper

Metal–Organic Frameworks

New s-Block Metal Pyridinedicarboxylate Network Structures through Gas-Phase Thin-Film Synthesis

Jenna Penttinen, Mikko Nisula, and Maarit Karppinen*[a]

Abstract: The combined atomic and molecular layer deposition (ALD/MLD) technique offers a unique way to build—both known and previously unknown—crystalline coordination polymer materials directly from gaseous precursors in a high-quality thin-film form. Here, we demonstrate the ALD/MLD of crystalline Li-, Na-, and K-based 3,5-pyridinedicarboxylate (3,5-PDC) thin films; the Li_2-3,5-PDC films are of the known Li-ULMOF-4 crystal structure whereas the other as-deposited crystalline films possess structures not previously reported. Another exciting possibility offered by ALD/MLD is the deposition of well-defined but amorphous metal–organic thin films, such as our Mg-, Ca-, Sr-, and Ba-based 3,5-PDC films, which can then be crystallized into water-containing structures through a post-deposition humidity treatment. All together, the new metal–organic structures realized in this study through ALD/MLD comprise a majority of the (anhydrous and water-containing) members of the s-block metal 3,5-pyridinedicarboxylate family.

Introduction

Coordination polymer (CP)-type metal–organic structures based on s-block metal centers and aromatic polycarboxylates as the organic linkers have attracted increasing interest as the electropositive alkali and alkaline earth metals form—compared to transition metals—stronger ionic bonds to the carboxylate oxygen atoms, thus providing us with exciting new chemistry features.[1–3] The open/porous structures expected for many of these materials make them promising material candidates for, for example, gas storage, sensors, smart membranes, and electrochemical electrodes; these structures could also serve as a new platform for non-native functionalities.

Pyridinedicarboxylic (PDC) acids are particularly interesting organic linker molecules with their rigid skeletons and multiple coordination sites, as they can act in a multidentate fashion, their N and O acceptors can participate in hydrogen-bonding interactions, and they may also exhibit π–π interactions between the stacked benzene rings.[4–6] All of these intermolecular interactions play an important role in stabilizing the structure and forming the extended polymeric system. Depending on the relative positions of the pyridyl and carboxylate groups we may expect different network structures for these materials. For the first-row transition metals and lanthanides a variety of coordination schemes and topologies have been realized,[7–9] and in some cases with the most oxophilic lanthanides and alkaline earth metals the pyridyl-N has been interestingly observed to remain as a non-coordinated freely accessible Lewis basic site within the porous framework.[10–14]

In case of the s-block metals, whereas for example, the 1,4-benzenedicarboxylate or so-called terephthalate (TP) structures have been well investigated,[15,16] with the highly symmetrical 3,5-PDC acid only the lithium 3,5-pyridinedicarboxylate (Li_2-3,5-PDC) structure has been realized through conventional solvothermal synthesis (without incorporated water molecules). Interestingly, although all the alkali and alkaline earth metal terephthalates have layered crystal structures, Li_2-3,5-PDC has—owing to the higher degree of freedom for possible coordination modes provided by the involvement of the pyridyl nitrogen—a 3D network structure, named Li-ULMOF-4 (ULMOF stands for ultra-light metal–organic framework, see Figure 1).[17]

For Na, Mg, Ca, Sr, and Ba solvothermal synthesis has yielded water-containing metal-3,5-PDC CP-type structures (see Figure 1 for representative examples).[4–6,18–23] This is in line with the general observation that the s-block metal-based CP structures are more prone to absorb guest water molecules than, for example, the transition-metal-based structures.[24–27] Furthermore, due to the ionic network, they are more flexible to rearrange their crystal structures from one crystal structure to another, for example, upon intercalation/deintercalation of coordinated water/solvent molecules.[12,28]

A viable assumption is that solvent-free conditions could promote the synthesis of anhydrous metal pyridinedicarboxylate network structures, and in this work, we demonstrate that this is indeed true. We employ the strongly emerging atomic/molecular layer deposition (ALD/MLD) thin-film technique[29,30] for the direct single-step synthesis of novel alkali and alkaline earth metal pyridinedicarboxylate materials. The combined ALD/MLD technique is—like its parent commercially well-established ALD technology[31]—based on self-limiting gas-surface reactions of alternating pulsed gaseous precursors. This

[a] J. Penttinen, M. Nisula, Prof. M. Karppinen
Department of Chemistry and Materials Science
Aalto University, 00076, Aalto (Finland)
E-mail: maarit.karppinen@aalto.fi
The ORCID identification number(s) for the author(s) of this article can be found under:
https://doi.org/10.1002/chem.201901034.

© 2019 Wiley-VCH Verlag GmbH & Co. KGaA, Weinheim

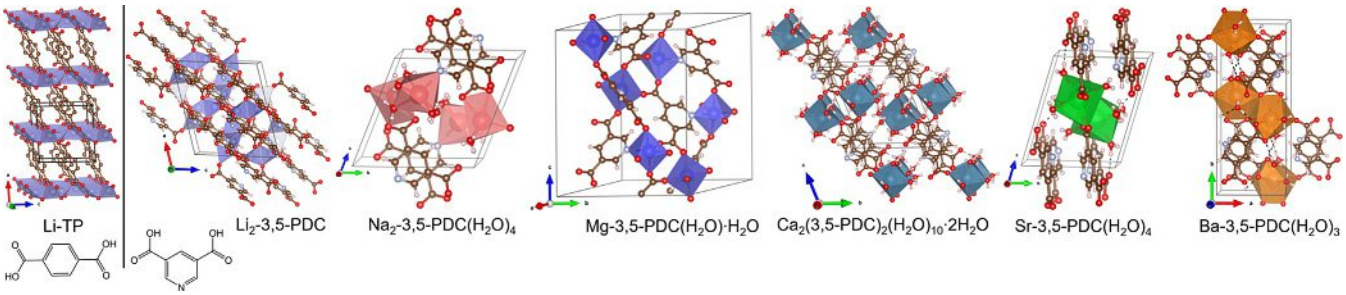

Figure 1. Some of the crystalline CP/MOF structures so far identified in solution-synthesized bulk samples for s-block metal 3,5-pyridinedicarboxylates: Li_2-3,5-PDC (and Li_2-TP for comparison) and the water-containing Na-, Mg-, Ca-, Sr-, and Ba-based 3,5-pyridinedicarboxylates;[4–6,15,17–19] structures drawn by using the VESTA[32] software. These representative structures were chosen as they turned out to be the most probable candidates to explain the crystal structures of our atomic and molecular layer deposition (ALD/MLD) thin-film materials.

enables the large-area uniformity and precise thickness control of the resultant thin films. The difference between ALD and MLD is in the precursors; in ALD the precursors are inorganic (metal complexes, water, ammonia, etc.), whereas in MLD they are purely organic. In ALD/MLD the deposition cycle consists of sequential pulses of a metal-containing precursor and an organic precursor to yield hybrid metal–organic thin films with an atomic/molecular level accuracy.

New ALD/MLD processes have been actively developed for a decade, but up until a few years ago it seemed that the technique was only capable to yield amorphous metal–organic thin films.[29,30] Initially, efforts were made to apply different post-deposition treatments to crystallize CP-type metal–organic structures from amorphous as-deposited films,[33–35] but three years ago we succeeded in growing the first in situ crystalline ALD/MLD metal–organic thin films.[36–44] In particular and most relevant to the present work, we recently fabricated a series of crystalline s-block metal-based terephthalate thin films with "sheet-like" ordered structures through ALD/MLD, and investigated their water-intercalation characteristics.[36,38,41,42] Now in the present work, we challenge for the first time s-block metal–PDC materials with the anticipation to discover novel CP-type structures. Moreover, fabricating these structures (with even so-called open metal sites for enhanced guest molecule absorption[45–47]) by using the industry-feasible ALD/MLD technique could be an important step along the roadmap towards devices based on new exciting metal–organic materials for, for example, microelectronics and sensing applications.[3,48]

Results and Discussion

We investigated the pyridinedicarboxylic acid ALD/MLD processes for the following s-block metal (M) components: Li, Na, K, Mg, Ca, Sr, and Ba; in each case the corresponding M(thd) (thd = 2,2,6,6-tetramethyl-3,5-heptanedione) complex was used as the metal precursor and most of the depositions were carried out at 220 °C; the metal precursor and the deposition temperature were taken from our previous ALD/MLD work on the M(thd)+TPA (TPA = terephthalic acid) processes[41] to enable the straightforward comparison. However, it should be mentioned that we carried out a number of additional depositions at different temperatures to confirm that the main conclusions, for example, for the crystallinity of the films remained the same independent of the deposition temperature used.

First of all, the Li(thd)+3,5-PDC process was found to yield highly crystalline thin films for which the grazing incidence X-ray diffraction (GIXRD) pattern (Figure 2) could be readily indexed according to the Li-ULMOF-4 structure reported for bulk Li_2-3,5-PDC samples. In Figure 2 we also re-plot a representative GIXRD pattern for our previously reported Li_2-TP films for comparison, to show that the diffraction pattern for the present films grown with the Li(thd)+3,5-PDC process consists of more diffraction peaks; we tentatively interpret this as an indication of a lower symmetry.

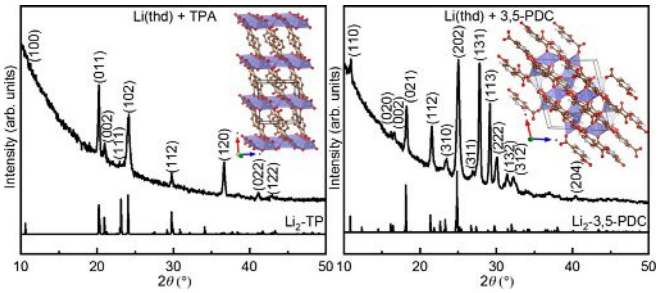

Figure 2. GIXRD patterns for thin films deposited at 220 °C with the Li(thd)+TPA (for comparison) and Li(thd)+3,5-PDC processes. The calculated patterns below the measured ones were produced from the reported crystal structures by using the VESTA[28] software.[15,17]

All the other M(thd)+3,5-PDC processes were also found to yield homogeneous thin films, but not necessarily in situ crystalline, see the GIXRD patterns in Figure 3. Crystalline films were obtained (besides Li) with Na and K, whereas those with Mg, Ca, Sr, and Ba were amorphous. In Figure 3, we also display the FTIR spectra for the same as-deposited thin films. For the K-based film a broad band is seen around $\tilde{\nu} = 3400\ cm^{-1}$, indicative of incorporated water. Apparently the as-deposited K-based films absorb water extremely rapidly in open air, forming an unknown crystalline water-containing structure. To be able to verify the anhydrous phase, we additionally deposited K(thd)+3,5-PDC films with a subsequently ALD-grown 4 nm thick Al_2O_3 capping layer to prevent the immediate water ab-

© 2019 Wiley-VCH Verlag GmbH & Co. KGaA, Weinheim

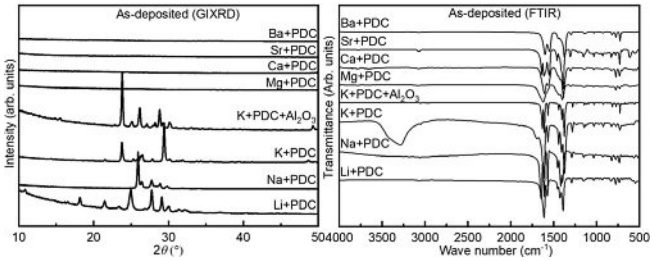

Figure 3. GIXRD patterns and FTIR spectra for thin films grown at 220 °C with the different M(thd)+3,5-PDC processes. In the case of M = K, films were also deposited with a 4 nm thick Al_2O_3 capping layer to prevent the immediate water absorption.

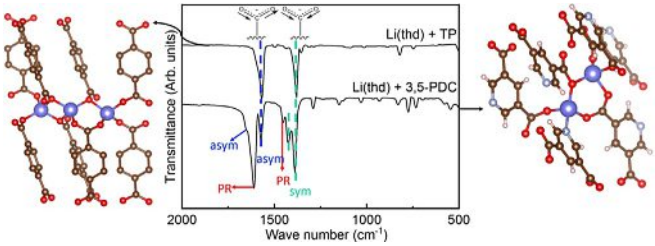

Figure 4. Comparison of the FTIR spectra recorded for as-deposited Li_2-TP and Li_2-3,5-PDC thin films; in the latter spectrum—besides the symmetric and asymmetric carboxylate peaks—features due to the pyridyl nitrogen (PR) participating in the metal coordination are seen.[15,17]

sorption of the hybrid film. In Figure 3, the GIXRD and FTIR data are shown for such an Al_2O_3-capped film as well; indeed, the FTIR spectrum does not show any indication of absorbed water and the GIXRD pattern reveals that the anhydrous phase is crystalline too, but with a structure different from that seen for the water-containing films. In literature, no anhydrous Na- or K-based pyridinedicarboxylate structures have been reported. Hence, we could conclude that our ALD/MLD processes have the capacity to yield thin films of new alkali metal 3,5-PDC network structures. Unfortunately, based on the GIXRD data only, it is not possible to solve such unknown/new metal–organic crystal structures. In the case of the Na-based film—as will be discussed in detail later—the GIXRD pattern resembles the one calculated from the reported crystal structure of the water-containing Na_2-PDC$(H_2O)_4$ compound previously synthesized in bulk form through solvothermal synthesis.[4]

Although we were unable to solve the crystal structures of the new alkali metal 3,5-PDC phases based on the GIXRD data, it was possible to address the bonding structures in these phases on the bases of the FTIR spectra shown in Figure 3. Firstly, we note that for all our M-3,5-PDC thin films (except for the un-capped K-3,5-PDC film, which contains post-deposition absorbed water) the region around $\tilde{\nu} = 1720\ cm^{-1}$ lacks the absorption band due to completely free COOH acid groups; this confirms that during the ALD/MLD process the dicarboxylic acid precursor reacts either with the metal species or with water molecules through hydrogen bonding. Then, the dominant absorption bands seen in all the spectra around $\tilde{\nu} = 1400$ and $1600\ cm^{-1}$ arise from the asymmetric and symmetric stretching vibrations of the carboxylate group, respectively. The broader COO^- bands seen for the Mg-, Ca-, Sr-, and Ba-based films in Figure 3 are consistent with the amorphous nature of these films (with more variation in the M–COO^- bonding),[49] whereas for the crystalline Li-, Na-, and K-based films the peaks are visibly sharper. Most importantly, the distance (Δ) between the two carboxylate absorption bands provides us an estimation about the bonding mode, as follows: for unidentate coordination $\Delta > 200\ cm^{-1}$, for bidentate chelating coordination $50 < \Delta < 150\ cm^{-1}$, and for bidentate bridging coordination $130 < \Delta < 200\ cm^{-1}$.[49,50] As an example, we compare in Figure 4 enlarged spectra for the two Li-based thin films of the known Li_2-3,5-PDC and Li_2-TP structures: for both of these films the Δ value ($146\ cm^{-1}$ for Li_2-3,5-PDC and $185\ cm^{-1}$ for Li_2-TP) is consistent with the bridging-type bonding in their crystal structures. In Table 1, we list the Δ values for all our thin-film samples; it can be seen that the as-deposited anhydrous films have either bidentate bridging or bidentate chelating coordination. The FTIR spectra moreover confirm the participation of the pyridyl-N entity in the metal coordination or in the hydrogen bonding with water molecules; the corresponding absorption feature is seen around $\tilde{\nu} = 1450\ cm^{-1}$, as indicated in Figure 4 in the case of Li_2-3,5-PDC.

Table 1. Summary of the FTIR data for all thin-film samples and the 3,5-PDC precursor: symmetric and asymmetric carboxylate bands (and the corresponding Δ values) and the N-bond absorption values given in cm^{-1}; b stands for a broad peak, f for a free pyridyl nitrogen/carboxylic acid, m for a metal coordinated to the pyridyl-N or a carboxylate, and h for a water molecule having hydrogen bonding to the pyridyl-N or to a carboxylate.

Sample	Sym	Asym	Δ	N bond
3,5-PDC	1304	1720	416 (f)	1421, 1602 (f)
Li-PDC	1425	1571	146 (m)	1450, 1610 (m)
	1390	1648	258 (m)	
Na-PDC	1417	1571	154 (m)	1454, 1614 (m)
	1396	1646	250 (m)	
Na-PDC-H_2O	1404	1547	143 (m)	1436, 1602 (m)
	1371	1666	295 (h)	
K-PDC	1403	1568	165 (m)	1442, 1607 (m)
	1374	1632	258 (m)	
K-PDC-H_2O	1407	1567	160 (m)	1442, 1614 (m)
	1371	1699	328 (h)	
Mg-PDC	1398 (b)	1569 (b)	171 (m)	1442, 1618 (m)
Mg-PDC-H_2O	1382	1562	180 (m)	1446, 1610 (m)
Ca-PDC	1386 (b)	1564 (b)	136 (m)	1454, 1609 (m)
Ca-PDC-H_2O	1432	1557	125 (m)	1452, 1601 (h)
	1389	1673	284 (h)	
Sr-PDC	1380 (b)	1556 (b)	129 (m)	1448, 1608 (m)
Sr-PDC-H_2O	1423	1552	170 (m)	1454, 1596 (h)
	1382	1614	232 (h)	
Ba-PDC	1376 (b)	1549 (b)	136 (m)	1448, 1601 (m)
Ba-PDC-H_2O	1378	1547	169 (m)	1448, 1601 (h)

Next, we discuss the water absorption behaviors of all the as-deposited (crystalline and amorphous) M(thd)+3,5-PDC thin films during an extended storage in open air (relative humidity (RH) = 30 %), and also upon applying a room-temperature humidity treatment under RH = 75 % conditions, followed by a subsequent thermal annealing in air (see Figure 5). Note that

© 2019 Wiley-VCH Verlag GmbH & Co. KGaA, Weinheim

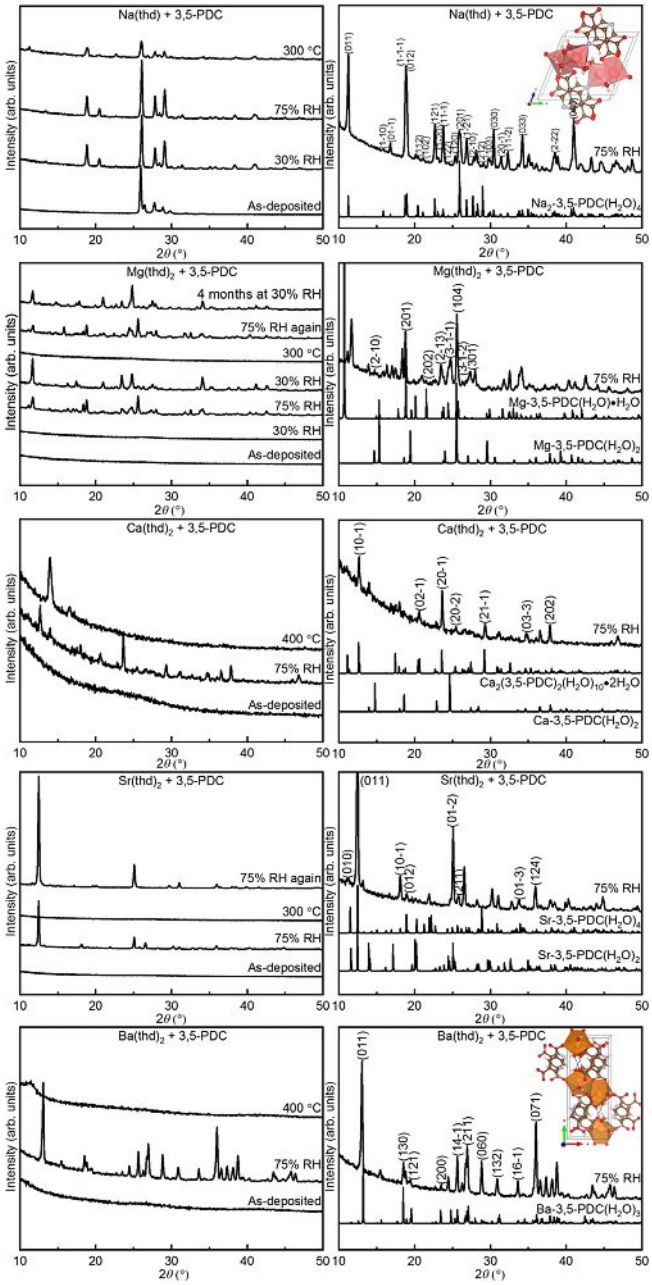

Figure 5. Left column) GIXRD patterns for variously treated thin films grown with the different M(thd)+3,5-PDC processes; the Ca-, Sr-, and Ba-based films behave similarly to the Mg-based one, and we therefore omit the RH = 30% data for them for the sake of simplicity. Right column) Comparison of the GIXRD patterns of the humidity-treated samples with all accessible diffraction data for the corresponding bulk samples,[4–6,18,20–23] and then indexed according to the literature data for which the closest resemblance is found (placed closest to the experimental pattern). It should be noted that the patterns shown here are for films grown with 200 ALD/MLD cycles except in the right-column Na(thd)+3,5-PDC case, where the data are for a thicker film grown with 1000 cycles (chosen in order to be able to verify even the weakest diffraction peaks).

from previous studies for the known water-containing s-block metal pyridinedicarboxylate bulk samples, the coordinated water molecules tend to detach upon heating in a continuous fashion in the temperature range of 70–225 °C, whereas the basic framework structures remain stable up to 500 °C or even beyond (before pyrolysis of the organic linker upon further heating).[4,17,20] Here, we carried out the heat treatments at 400 °C for the K-, Ca-, and Ba-based films and at 300 °C for the others.

For the Li_2-3,5-PDC films no changes in the GIXRD pattern were seen during the standard storage at approximately RH = 30% or upon the aforementioned humidity or heat treatments. This is in line with the data previously reported for bulk Li_2-3,5-PDC samples.[17] From the GIXRD data collected for the other samples after the different treatments (Figure 5), it can be seen that all the other samples experience some changes. For the Na-based films stored at RH = 30% or humidity-treated at RH = 75% the GIXRD patterns are consistent with the 3D water-containing Na_2-3,5-PDC$(H_2O)_4$ structure previously detected in bulk samples.[4] Comparison of the GIXRD patterns for our anhydrous and water-containing Na-based films reveals that the patterns are very similar but not entirely identical; the pattern for the watery film exhibits several additional peaks suggesting that the coordinated water adds some complexity to the crystal structure.

From Figure 5, the as-deposited amorphous Mg-, Ca-, Sr-, and Ba-based films are all found to crystallize upon the humidity treatment; then when the films are heat treated they become amorphous (or nearly amorphous in the case of Ca and Ba) again, implying that the coordinated water molecules are apparently needed to satisfy the coordination requirement of the corresponding crystalline networks. The GIXRD pattern for the hydrated Ba-based film is essentially compatible with the known Ba-3,5-PDC$(H_2O)_3$ having a 2D structure,[6] whereas the GIXRD patterns for the hydrated Mg-, Ca-, and Sr-based films are somewhat different from those expected for the Mg-3,5-PDC(H_2O)·H_2O (3D), Mg-3,5-PDC$(H_2O)_2$ (2D), Ca-(3,5-PDC)$_2(H_2O)_{10}$·2H_2O (0D), Ca-3,5-PDC$(H_2O)_2$ (2D), Sr-3,5-PDC$(H_2O)_2$ (2D), and Sr-3,5-PDC$(H_2O)_4$ (1D) structures known from bulk samples.[5,18–20,22,23] This is not strange, as the binding mode and coordination number are likely to depend on the amount of coordinated water; this is at least what has been reported for water-containing strontium terephthalate bulk samples (possessing mono-, tri-, and tetrahydrated structures besides the anhydrous structure)[51] and for water-containing strontium 3,5-PDC bulk samples (possessing di- and tetrahydrated structures).[5,23] It should also be mentioned that the water-containing Mg-, Ca-, Sr-, and Ba-based structures found in our thin films remain crystalline even at low-humidity conditions once formed under the high-humidity conditions. On the other hand, the as-deposited amorphous films do not absorb enough water to turn into crystalline form during storage at RH = 30%, and the watery structures obtained after treating the film at RH = 75% again lose the absorbed water (and become amorphous) when being heat treated at 300–400 °C. We moreover confirmed that these reversible water absorption/desorption-derived changes could be repeated several times without breaking the basic metal–organic structure, as illustrated for the Mg- and Sr-based films in Figure 5.

We used FTIR measurements—like for the as-deposited films—to investigate the bonding schemes in our hydrated thin films. The data confirmed the expected absorption bands

© 2019 Wiley-VCH Verlag GmbH & Co. KGaA, Weinheim

arising from OH^- groups in the $\tilde{\nu}=3400\ cm^{-1}$ region for all our hydrated thin films (not shown here). For the Na-based film we could nicely corroborate the expected Na_2-3,5-PDC$(H_2O)_4$ structure (see Figure 6). The two strong absorption peaks at $\tilde{\nu}=3457$ and $3390\ cm^{-1}$ are due to the ν(O–H) vibrations of the terminal and μ_2-bridging-type coordinated water molecules, whereas the absorption bands at $\tilde{\nu}=1547$ and $1404\ cm^{-1}$ arise from the asymmetric and symmetric stretching vibrations of the carboxylate group, respectively, in line with the spectra reported for bulk Na_2-3,5-PDC$(H_2O)_4$ samples.[4] The Δ value ($143\ cm^{-1}$) for our thin-film sample implies towards a bridging bonding mode. However, the carboxylate peaks are split,[46,50] such that there is another set of peaks at $\tilde{\nu}=1666$ and $1371\ cm^{-1}$ with $\Delta=295\ cm^{-1}$. This second Δ value indicates towards "free" carboxylic acid; in this case there are O–H···O–H-bonds between hydrogen atoms from four water molecules and carboxylic oxygen atoms.[4]

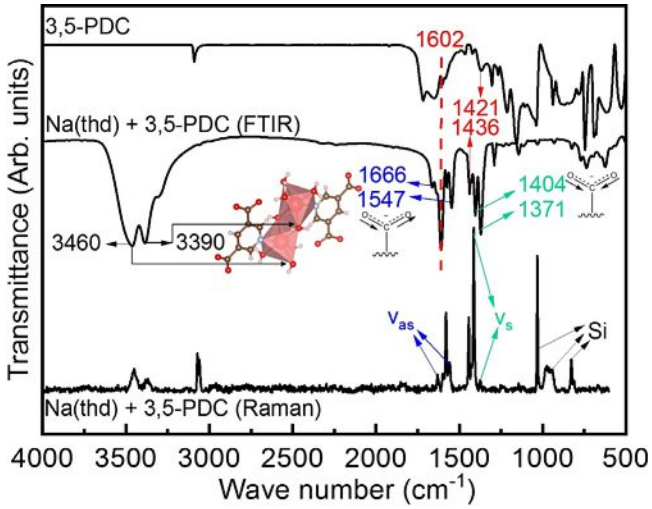

Figure 6. FTIR and Raman spectra for a hydrated Na-based thin film together with an FTIR spectrum for the 3,5-PDC precursor powder for comparison. The FTIR data are interpreted based on the known Na_2-3,5-PDC$(H_2O)_4$ structure.[4]

The asymmetric and symmetric vibrations of the carboxylate group and the absence of completely free carboxylic acid could also be confirmed from a Raman spectrum measured for the same sample (Figure 6). Finally, the shift in the position of the pyridine-ring (PR) stretching band to higher wavenumbers, from $\tilde{\nu}=1421\ cm^{-1}$ for the 3,5-PDC precursor to $\tilde{\nu}=1436\ cm^{-1}$ for the hydrated Na(thd)+3,5-PDC film can be interpreted as an indication of the pyridine-N coordination to the Na^+ ion.[52,53] Another PR stretching is seen at approximately $\tilde{\nu}=1602\ cm^{-1}$ for both the thin film and the 3,5-PDC precursor. Also, around $\tilde{\nu}=1577\ cm^{-1}$ a weaker vibration band refers to a conjugated PR due to the weaker aromaticity of the salt.[53]

We summarize our FTIR findings for all the samples, both anhydrous and water-containing, in Table 1. For some of the samples, the carboxylate entity possesses two different coordination modes, seen as two different Δ values were found. The smaller Δ value originates from a more tightly bound carboxylate, whereas the larger Δ value refers to a more loosely bound carboxylate.[50] Some of the structures lack the second wider peak separation, indicating that both carboxylic acids in the 3,5-PDC are coordinated to metal centers in an essentially similar way. For the amorphous thin-film samples the peak positions are not accurate due to the broader COO^- bands.

We employed both optical and scanning electron microscopy to investigate the morphologies in our metal–organic thin films. Here, we show in Figure 7 as an example, images for the Mg- and Sr-based thin films before and after a humidity treatment. The amorphous anhydrous films have seemingly smoother film surfaces (Figure 7a) compared to the crystalline water-containing films that have observable shapes due to crystallization. The crystalline Mg-based film has a more continuous and granular morphology (Figure 7b), whereas the crystals in the Sr-based film are more clearly visible (Figure 7c).

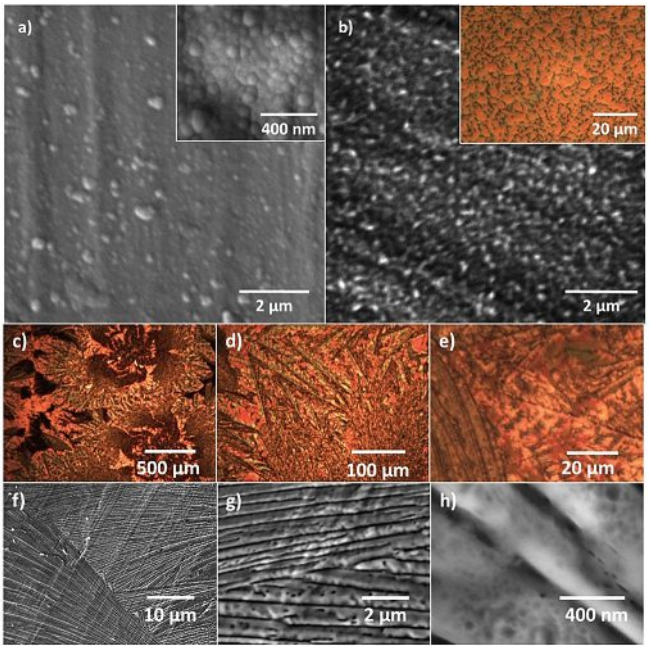

Figure 7. Top row) SEM images for amorphous anhydrous (left) and crystalline (right) water-containing Mg-based films. Inserts show the same sample with different scale measured with SEM (a) and optical microscope (b). Middle row) Optical microscope images for a crystalline water-containing Sr-based film. Bottom row) SEM images for the same sample.

Finally, we investigated the deposition parameters and confirmed the expected controllability of our new ALD/MLD processes based on the metal–thd and 3,5-PDC precursors. Most systematic experiments were carried out for the $Mg(thd)_2$+3,5-PDC process; in the following we hence report these results in detail. Initially, we fixed the deposition temperature to 220 °C and the number of ALD/MLD cycles to 200, and investigated the growth-per-cycle (GPC) values as a function of the precursor pulse lengths. The GPC values were calculated from the X-ray reflectivity (XRR)-determined film thickness values; an example of a typical XRR curve is shown in the inset of Figure 8c. From Figure 8b it can be seen that the GPC value is well saturated when the $Mg(thd)_2$ pulse length is 5 s (subsequent N_2

© 2019 Wiley-VCH Verlag GmbH & Co. KGaA, Weinheim

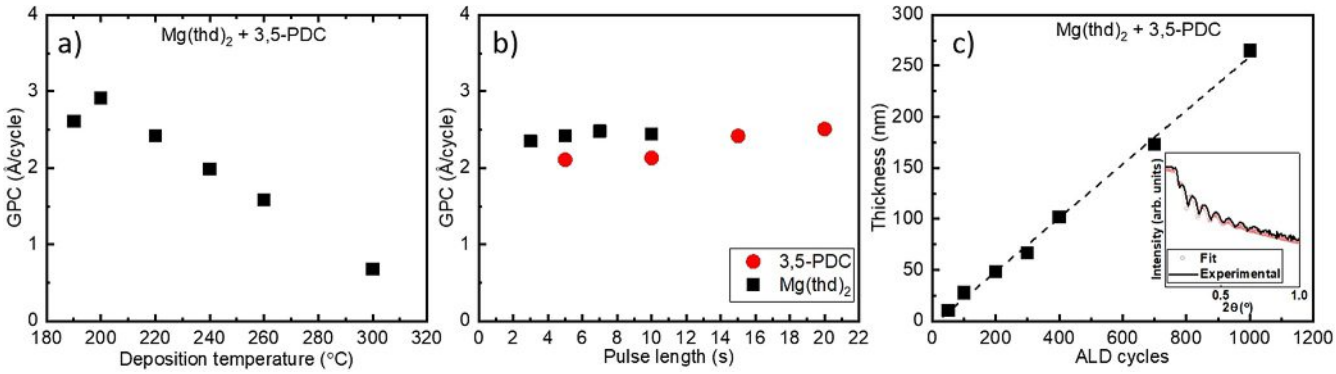

Figure 8. GPC values for the $Mg(thd)_2$+3,5-PDC process as a function of a) the deposition temperature and b) the precursor pulse lengths. c) Thickness of the films as function of the number of ALD/MLD cycles (the inset shows an experimental XRR pattern and its fitting for a film with 300 cycles). The deposition temperature was 220 °C, the number of ALD/MLD cycles was 200 (in a and b), and the metal/3,5-PDC precursor pulse lengths were 5 s/15 s (in a and c).

purge length 5 s) and the 3,5-PDC precursor pulse length is 15 s (subsequent N_2 purge length 30 s). It should be mentioned that very similar pulse length values are typically used for many other organic precursors in ALD/MLD processes.[29,41] We then fixed these pulse/purge lengths for the rest of the experiments. From Figure 8a can then be seen that with increasing deposition temperature the film growth rate decreases, which is also a common feature with carboxylic acid precursors in ALD/MLD.[41,54,55] The expected fact that the film thickness increases with the number of ALD/MLD cycles applied is seen from Figure 8c.

Our new ALD/MLD M(thd)+3,5-PDC processes worked in an essentially similar manner for all the s-block metal constituents. The GPC values for the Li-, Na-, and K-based processes were 2.5, 3.7, and 3.5 Å per cycle, respectively, and for the Mg-, Ca-, Sr-, and Ba-based processes 2.4, 3.7, 4.2, and 3.6 Å per cycle, respectively. Apparently the possible in situ crystallinity of the growing film does not have any clear effect on the GPC value. In our previous study for the alkali and alkaline earth terephthalate thin films, the GPC values were essentially on the same level, that is, around 3 Å per cycle.[41] For amorphous Eu- and Er-based 3,5-PDC films, on the other hand, slightly lower GPC values in the range of 2.0–2.4 Å per cycle, were observed,[56–58] possibly due to the more pronounced steric hindrance by the three-ligand $Eu(thd)_3$ and $Er(thd)_3$ precursors.

Conclusion

We have demonstrated that coordination polymer thin films where the 3,5-pyridinedicarboxylate anion acts as the organic linker can be fabricated in a single-step process from gaseous precursors for most of the members of the s-block metal family. For the alkali metals the as-deposited anhydrous films were crystalline, whereas for the alkaline earth metals they were amorphous. The remarkable fact to note is that prior to the present work, only the Li_2-3,5-PDC compound was known among the water-free structures. Our results thus underline the important role of solution-free conditions for the stabilization of anhydrous metal–organic framework structures.

We also extensively investigated the post-deposition water-absorption behaviors of our new ALD/MLD metal–organic thin films, both the crystalline and amorphous ones. Intercalation of water or other guest species is of major issue—either positive or negative—for many of the potential future applications of the coordination-network materials in, for example, electronics, sensors, and other high-tech products. Equally important is to understand the water intercalation characteristics from the fundamental chemistry point of view, in particular for the s-block metal-based structures with relatively ionic bonds. Here, among our as-deposited anhydrous M-3,5-PDC thin films all, except the Li-based film, were found to absorb water to form crystalline—either known or unknown—water-containing M-3,5-PDC phases. Although the new crystal structures could not be addressed based on the GIXRD data, we were nevertheless able to discuss the bonding structures in these new materials based on our systematic FTIR data.

Finally, we summarize in Figure 9 all the anhydrous and water-containing M-3,5-PDC thin-film phases realized—both amorphous and crystalline—together with the corresponding M-TPA phases for comparison. Having now so many members of these four families synthesized, it would be interesting to start to look for possible trends in their properties. Here, we determined the densities for all these materials from the XRR data (Figure 9). Two observations are immediate: firstly, for all the metal constituents, water absorption decreases the density; secondly, compared to the corresponding TPA phases the 3,5-PDC phases are less dense (Sr being the only exception).

Experimental Section

Thin-film deposition: In our ALD/MLD processes we employed metal-thd complexes (thd = 2,2,6,6-tetramethyl-3,5-heptanedione; synthesized in-house) as metal precursors and 3,5-pyridinedicarboxylic acid (3,5-PDC; Tokyo Chemical Industry CO., Ltd. 98.0% purity) as the organic precursor. The depositions were carried out in a commercial flow-type hot-wall ALD reactor (F-120 by ASM Microchemistry Ltd). The solid precursors were kept in open glass crucibles inside the reactor. The reactor pressure was approximate-

© 2019 Wiley-VCH Verlag GmbH & Co. KGaA, Weinheim

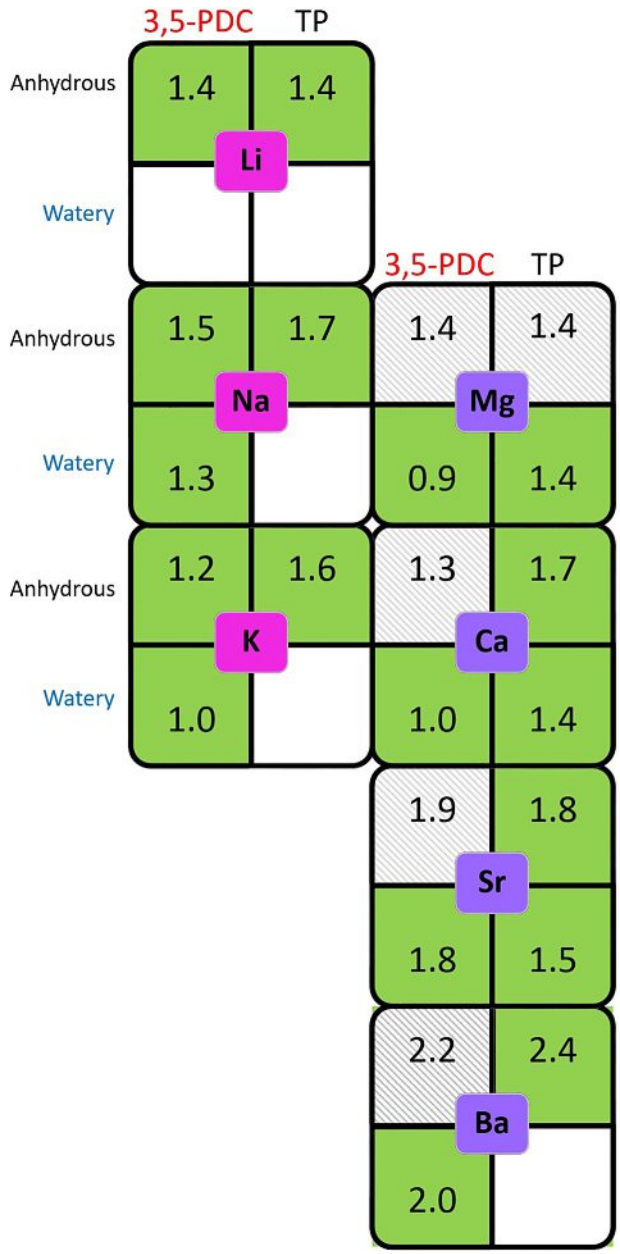

Figure 9. Summary of the s-block metal 3,5-PDC films realized in this study, and the corresponding TPA thin films reported earlier:[41] crystalline films are indicated in green and amorphous films in striped gray. We also give the density values (in g cm^{-3}) determined for each thin-film sample from the critical angle value in the XRR pattern.

ly 3 mbar and nitrogen (99.999%; Parker HPN 5000 N_2 generator) was used both as the purging and carrier gas.

The thin films were deposited on Si(100) substrates (3.0×3.0 cm^2), initially at different temperatures in the range of 190–300 °C depending of the precursor used. The sublimation temperatures were 175, 180, 220, 115, 198, 180, and 210 °C for Li(thd), Na(thd), K(thd), Mg(thd)$_2$, Ca(thd)$_2$, Sr(thd)$_2$, and Ba(thd)$_2$, respectively, and 190 °C for 3,5-PDC. For the final comparative investigations, all the deposition processes were conducted at 220 °C, because this temperature was found suitable for all the processes and it was from the lower side of the temperature range. The pulse/purge lengths for the inorganic precursor pulses were 4 s/4 s for Li(thd), Na(thd), and K(thd) and 5 s/5 s for Mg(thd)$_2$, Ca(thd)$_2$, Sr(thd)$_2$, and Ba(thd)$_2$. The 3,5-PDC pulse/purge length was 15 s/30 s for all processes. The capping layer of 4 nm thick Al_2O_3 was deposited (on some humidity-sensitive films) with 2 s/2 s TMA (TMA = trimethylaluminum) and 2 s/5 s H_2O pulse/purge with 40 cycles at 150 °C.

Characterization: The crystallinity/crystal structure was confirmed for the films by using grazing incidence X-ray diffraction (X'Pert Pro, PANalytical; $Cu_{K\alpha}$) measurements. The film thickness and density were determined through X-ray reflectivity measurements by using the same equipment. In the measurements, the time per step was set at 20 and 6 s in GIXRD and XRR, respectively, and in the GIXRD measurements, an incidence angle of 0.5° was used. The film thickness values were determined from the averages of the values calculated by using the direct calculation and the Fourier methods. For some of the samples (in particular those with some surface adsorption/absorption of water) the XRR data were fitted with the X'Pert Reflectivity software by using a multilayer model. For the thickest films (>100 nm) the thicknesses were determined with spectroscopic ellipsometer measurements with a Woollam spectroscopic ellipsometer by using the CompleteEASE software for data analysis. The density of the films was deduced from the critical angle θ_c in the XRR patterns, as follows: $\rho_e = (\theta_c^2\pi)/(\lambda^2 r_e)$, in which ρ_e is the mean electron density, λ is the X-ray wavelength, and r_e is the classical electron radius. By assuming the elemental composition being that of pure alkali/alkaline earth metal-3,5-PDC, that is, $M_2C_7H_3O_4N(H_2O)_n/MC_7H_3O_4N(H_2O)_n$, the mass density was estimated from $\rho_m = (\rho_e A)/(N_A Z)$, where A is the average molar mass, N_A is the Avogadro constant, and Z is the average atomic number.

The morphology of the films was investigated with an Euromex optical microscope having a fiber optic light source EK-1 and by scanning electron microscopy (SEM) with a Tescan Mira3 with a Schottky emitter. The SEM images were recorded by utilizing a secondary electron detector. A low voltage of 5 kV was used due to the sensitivity of the samples. The SEM samples were coated with 5 nm 80/20 Au/Pd.

The chemical composition/bonding was studied by Fourier transform infrared spectroscopy. The measurements were carried out in a transmission mode with a Nicolet Magna 750 spectrometer in the range of $\tilde{\nu}$ = 400–4000 cm^{-1} by using a resolution of 4 cm^{-1} and analyzed from 32 measured spectra. A spectrum of blank Si was subtracted from the spectra to compensate for the effect of the substrate. Raman spectra were obtained by using a Horiba Jobin–Yvon Labram HR Raman spectrometer with an Ar ion laser with a wavelength of λ = 514 nm as the light source.

The water absorption/desorption characteristics of the films were investigated with humidity and heat treatments. In the humidity treatments, the thin-film sample was stored in a glass box with concentrated salt solution (NaCl) that gives 75% relative humidity (RH). The relative humidity of the laboratory air was approximately 30%. In the thermal treatment tests, the sample was heat treated in a muffle furnace (Nabertherm LT 9/11) in air at 300–400 °C for fifteen minutes.

Acknowledgements

The present work has received funding from the European Research Council under the European Union's Seventh Framework Programme (FP/2007-2013)/ERC Advanced Grant Agreement (No. 339478) and the Academy of Finland (Nos. 296299 and 303452), and made use of the RawMatTERS Finland infrastructure (RAMI) and Aalto Nanomicroscopy Center (Aalto

© 2019 Wiley-VCH Verlag GmbH & Co. KGaA, Weinheim

NMC) facilities based at Aalto University. J.Heiska is thanked for carrying out the SEM measurements.

Conflict of interest

The authors declare no conflict of interest.

Keywords: alkaline metals · alkaline earth metals · atomic layer deposition · metal–organic frameworks · molecular layer deposition · thin films

[1] J. L. C. Rowsell, O. M. Yaghi, *Microporous Mesoporous Mater.* **2004**, *73*, 3–14.
[2] D. Banerjee, J. B. Parise, *Cryst. Growth Des.* **2011**, *11*, 4704–4720.
[3] J. Lei, R. Qian, P. Ling, L. Cui, H. Ju, *TrAC Trends Anal. Chem.* **2014**, *58*, 71–78.
[4] W. Huang, X. Xie, K. Cui, S. Gou, Y. Li, *Inorg. Chim. Acta* **2005**, *358*, 875–884.
[5] H. Aghabozorg, A. Nemati, Z. Derikvand, M. Ghadermazi, S. Daneshvar, *Acta Crystallogr. Sect. E* **2008**, *64*, m376–m376.
[6] H. Aghabozorg, A. Nemati, Z. Derikvand, M. Ghadermazi, S. Daneshvar, *Acta Crystallogr. Sect. E* **2008**, *64*, m375–m375.
[7] H. Xu, N. Zheng, H. Xu, Y. Wu, R. Yang, E. Ye, X. Jin, *J. Mol. Struct.* **2002**, *606*, 117–122.
[8] Y. L. Lu, J. Y. Wu, M. C. Chan, S. M. Huang, C. S. Lin, T. W. Chiu, Y. H. Liu, Y. S. Wen, C. H. Ueng, T. M. Chin, C.-H. Hung, K.-L. Lu, *Inorg. Chem.* **2006**, *45*, 2430–2437.
[9] S. K. Ghosh, P. K. Bharadwaj, *Inorg. Chem.* **2005**, *44*, 3156–3161.
[10] G. Nandi, H. M. Titi, R. Thakuria, I. Goldberg, *Cryst. Growth Des.* **2014**, *14*, 2714–2719.
[11] B. Chen, L. Wang, Y. Xiao, F. R. Fronczek, M. Xue, Y. Cui, G. Qian, *Angew. Chem. Int. Ed.* **2009**, *48*, 500–503; *Angew. Chem.* **2009**, *121*, 508–511.
[12] J. Jia, X. Lin, A. J. Blake, N. R. Champness, P. Hubberstey, L. Shao, G. Walker, C. Wilson, M. Schröder, *Inorg. Chem.* **2006**, *45*, 8838–8840.
[13] Y. Chen, S. Ma, *Rev. Inorg. Chem.* **2012**, *32*, 81–100.
[14] Y. Kim, S. Huh, *CrystEngComm* **2016**, *18*, 3524–3550.
[15] J. A. Kaduk, *Acta Crystallogr. Sect. B* **2000**, *56*, 474–485.
[16] J. A. Kaduk, *Acta Crystallogr. Sect. B* **2002**, *58*, 815–822.
[17] D. Banerjee, S. J. Kim, L. A. Borkowski, W. Xu, J. B. Parise, *Cryst. Growth Des.* **2010**, *10*, 709–715.
[18] A. Mallick, S. Saha, P. Pachfule, S. Roy, R. Banerjee, *J. Mater. Chem.* **2010**, *20*, 9073–9080.
[19] W. Starosta, H. Ptasiewicz-Bąk, J. Leciejewicz, *J. Coord. Chem.* **2002**, *55*, 1–9.
[20] D. Banerjee, J. Finkelstein, A. Smirnov, P. M. Forster, L. A. Borkowski, S. J. Teat, J. B. Parise, *Cryst. Growth Des.* **2011**, *11*, 2572–2579.
[21] W. Starosta, H. Ptasiewicz-Bąk, J. Leciejewicz, *J. Coord. Chem.* **2002**, *55*, 985–990.
[22] A. M. Plonka, D. Banerjee, J. B. Parise, *Cryst. Growth Des.* **2012**, *12*, 2460–2467.
[23] D. Li, C. Duan, *Acta Crystallogr. Sect. E* **2012**, *68*, m835–m835.
[24] A. C. Kizzie, A. G. Wong-Foy, A. J. Matzger, *Langmuir* **2011**, *27*, 6368–6373.
[25] K. M. Fromm, *Coord. Chem. Rev.* **2008**, *252*, 856–885.
[26] L. Wang, C. Mou, Y. Sun, W. Liu, Q. Deng, J. Li, *Electrochim. Acta* **2015**, *173*, 235–241.
[27] G. Scholz, F. Emmerling, M. Dreger, E. Kemnitz, *Z. Anorg. Allg. Chem.* **2013**, *639*, 689–693.
[28] B. F. Abrahams, A. D. Dharma, M. J. Grannas, T. A. Hudson, H. E. Maynard-Casely, G. R. Oliver, R. Robson, K. F. White, *Inorg. Chem.* **2014**, *53*, 4956–4969.
[29] P. Sundberg, M. Karppinen, *Beilstein J. Nanotechnol.* **2014**, *5*, 1104–1136.
[30] K. B. Klepper, O. Nilsen, H. Fjellvåg, *Dalton Trans.* **2010**, *39*, 11628–11635.
[31] S. M. George, *Chem. Rev.* **2010**, *110*, 111–131.
[32] K. Momma, F. Izumi, *J. Appl. Crystallogr.* **2011**, *44*, 1272–1276.
[33] L. D. Salmi, M. J. Heikkilä, E. Puukilainen, T. Sajavaara, D. Grosso, M. Ritala, *Microporous Mesoporous Mater.* **2013**, *182*, 147–154.
[34] L. D. Salmi, M. J. Heikkilä, M. Vehkamäki, E. Puukilainen, M. Ritala, T. Sajavaara, *J. Vac. Sci. Technol. A* **2015**, *33*, 01A121.
[35] K. B. Lausund, O. Nilsen, *Nat. Commun.* **2016**, *7*, 13578.
[36] E. Ahvenniemi, M. Karppinen, *Chem. Commun.* **2016**, *52*, 1139–1142.
[37] E. Ahvenniemi, M. Karppinen, *Chem. Mater.* **2016**, *28*, 6260–6265.
[38] M. Nisula, M. Karppinen, *Nano Lett.* **2016**, *16*, 1276–1281.
[39] M. Nisula, J. Linnera, A. J. Karttunen, M. Karppinen, *Chem. Eur. J.* **2017**, *23*, 2988–2992.
[40] Z. Giedraityte, O. Lopez-Acevedo, L. A. Espinosa Leal, V. Pale, J. Sainio, T. S. Tripathi, M. Karppinen, *J. Phys. Chem. C* **2016**, *120*, 26342–26349.
[41] J. Penttinen, M. Nisula, M. Karppinen, *Chem. Eur. J.* **2017**, *23*, 18225–18231.
[42] A. Tanskanen, M. Karppinen, *Sci. Rep.* **2018**, *8*, 8976.
[43] Z. Giedraityte, J. Sainio, D. Hagen, M. Karppinen, *J. Phys. Chem. C* **2017**, *121*, 17538–17545.
[44] V. Pale, Z. Giedraityte, X. Chen, O. Lopez-Acevedo, I. Tittonen, M. Karppinen, *Sci. Rep.* **2017**, *7*, 6982.
[45] L. E. Kreno, K. Leong, O. K. Farha, M. Allendorf, R. P. Van Duyne, J. T. Hupp, *Chem. Rev.* **2012**, *112*, 1105–1125.
[46] I. Stassen, D. De Vos, R. Ameloot, *Chem. Eur. J.* **2016**, *22*, 14452–14460.
[47] D. Zacher, O. Shekhah, C. Wöll, R. A. Fischer, *Chem. Soc. Rev.* **2009**, *38*, 1418–1429.
[48] M. D. Allendorf, A. Schwartzberg, V. Stavila, A. A. Talin, *Chem. Eur. J.* **2011**, *17*, 11372–11388.
[49] K. B. Klepper, O. Nilsen, S. Francis, H. Fjellvåg, *Dalton Trans.* **2014**, *43*, 3492–3500.
[50] G. B. Deacon, R. J. Phillips, *Coord. Chem. Rev.* **1980**, *33*, 227–250.
[51] M. Ghazzali, M. Khair, K. Al-Farhan, J. Reedijk, *Inorg. Chim. Acta* **2014**, *409*, 503–506.
[52] S. Akyüz, A. B. Dempster, R. L. Morehouse, S. Suzuki, *J. Mol. Struct.* **1973**, *17*, 105–125.
[53] M. Katcka, T. Urbanski, *Bull. Acad. Pol. Sci. Ser. Sci. Chim.* **1964**, *12*, 615–621.
[54] K. B. Klepper, O. Nilsen, T. Levy, H. Fjellvåg, *Eur. J. Inorg. Chem.* **2011**, *34*, 5305–5312.
[55] B. H. Lee, B. Yoon, A. I. Abdulagatov, R. A. Hall, S. M. George, *Adv. Funct. Mater.* **2013**, *23*, 532–546.
[56] L. Mai, Z. Giedraityte, M. Schmidt, D. Rogalla, S. Scholz, A. D. Wieck, A. Devi, M. Karppinen, *J. Mater. Sci.* **2017**, *52*, 6216–6224.
[57] Z. Giedraityte, P. Sundberg, M. Karppinen, *J. Mater. Chem. C* **2015**, *3*, 12316–12321.
[58] Z. Giedraityte, L.-S. Johansson, M. Karppinen, *RSC Adv.* **2016**, *6*, 103412–103417.

Manuscript received: March 5, 2019
Revised manuscript received: May 31, 2019
Accepted manuscript online: June 5, 2019
Version of record online: August 7, 2019

© 2019 Wiley-VCH Verlag GmbH & Co. KGaA, Weinheim